



INFN-16-08/GE

31<sup>st</sup> May 2016

**THERMAL ANALYSIS OF THE ANTINEUTRINO  $^{144}\text{Ce}$  SOURCE  
CALORIMETER FOR THE SOX EXPERIMENT**

Stefania Farinon<sup>1</sup>, Riccardo Musenich<sup>1</sup>, Marco Pallavicini<sup>1,2</sup>, Fabio Bragazzi<sup>1</sup>, Roberto Cereseto<sup>1</sup>, Alessio Caminata<sup>1</sup>, Lea Di Noto<sup>1</sup>, Paolo Saracco<sup>1</sup>, Cecilia Rossi<sup>1</sup>, Gemma Testera<sup>1</sup>, Sandra Zavatarelli<sup>1</sup>

<sup>1</sup>) *INFN-Sezione di Genova, Via Dodecaneso 33, 16146 Genova, Italy*

<sup>2</sup>) *Dipartimento di Fisica, Università di Genova, Via Dodecaneso 33, 16146 Genova, Italy*

**Abstract**

The technical note describes the calorimeter which will be used to measure the activity of the antineutrino  $^{144}\text{Ce}$  source of the SOX experiment at the Gran Sasso Laboratories. The principle of the calorimeter is based on the measurement of both mass flow and temperature increase of the water circulating in the heat exchanger surrounding the source. The calorimeter is vacuum insulated in order to minimize the heat losses. The preliminary design and thermal Finite Element Analysis (FEA) are reported in the note.

## 1 INTRODUCTION

The SOX experiment<sup>1</sup> aims at testing the long-standing issue of the existence of the sterile neutrinos. The existence of this type of neutrinos is suggested by the results of the LSND<sup>2</sup> and Miniboone<sup>3</sup> experiments, the results of the source calibration of the Gallex and Sage experiments<sup>4</sup> and the recently hinted reactor anomaly.<sup>5,6</sup> If the previous results are analyzed in the theoretical framework of sterile neutrinos (i.e. neutrinos that are not coupled with the  $Z^0$  boson and, therefore, do not interact weakly), they hint the existence of a sterile neutrino with a  $\Delta m$  of about one eV.<sup>7</sup>

It is possible to investigate the relevant region of the parameter space using neutrinos or anti-neutrinos produced in nuclear decays. This can be understood from the well-known two flavors oscillation formula:

$$P_{ee} = 2 \sin^2 2\vartheta_{14} \sin^2 \frac{1.27 \Delta m_{41}^2 (\text{eV}^2) L (\text{m})}{E (\text{MeV})} \quad (1)$$

where  $\vartheta_{14}$  is the mixing angle of the standard neutrino (or anti-neutrino) into sterile component,  $\Delta m_{41}^2$  is the corresponding squared mass difference,  $L$  is the distance of the source from the detection point and  $E$  is the particle energy. In case of nuclear decay, the typical energy is about 1 MeV and, to study sterile neutrinos with  $\Delta m_{41}^2$  of about 1 eV<sup>2</sup>, the source can be placed few meters away from the detector. The existence of sterile neutrinos can be proved looking for the disappearance of neutrinos emitted by the source and/or searching for oscillation waves within the detector volume.<sup>1</sup>

The SOX experiment aims at the detection of standard neutrinos emitted by a radioactive source positioned under the Borexino detector (INFN Gran Sasso National Laboratory, Italy). Due to the very low background, the large volume and the capability to detect low energy neutrinos<sup>8,9</sup> and anti-neutrinos,<sup>10</sup> Borexino is the ideal detector to investigate the existence of sterile neutrinos. The SOX collaboration selected an anti-neutrino source based on the decay of <sup>144</sup>Ce (<sup>144</sup>Ce → <sup>144</sup>Pr → <sup>144</sup>Nd). Neutrinos are detected in Borexino by means of elastic scattering on electrons while anti-neutrinos are detected via inverse beta decay. As the <sup>144</sup>Ce source is sealed into a massive radioprotection tungsten shield and consequently is inaccessible, the source activity will be measured by a calorimeter through an accurate measurement of the heat released by the source. In order to maximize the chance to achieve the required accuracy (<1%), both INFN and CEA are developing in parallel a water flow calorimeter to measure the activity of neutrino sources.

This technical note summarizes the thermal Finite Element Analysis (FEA) carried out on the cerium oxide source, which is scheduled to be the first to be measured. Data on the

source have been supplied by CEA.<sup>11</sup> The analyses have been performed using the FE software ANSYS.<sup>12</sup>

## 2 THE PRINCIPLE OF CALORIMETRIC MEASUREMENT

The heat rate produced by the nuclear reaction of the  $^{144}\text{Ce}$  source can be estimated via flow calorimetric measurements, i.e. by measuring the temperature increase of a flowing fluid. If the source is sealed within its biological shield which is surrounded by a heat exchanger and by a thermal insulation (see Fig. 1), in steady state conditions, the energy balance can be written as:

$$P_g = \int_{T_{in}}^{T_{out}} \dot{m}C(T)dT + \Delta P_b \quad (2)$$

where  $P_g$  is the power generated by the source,  $C$  is the specific heat capacity and  $\dot{m}$  is the fluid mass flow. The first term of the right member is the power transferred to the fluid while the second one,  $\Delta P_b$  contains the heat leak through the thermal insulation (a positive term) and the spuriously generated power (negative), mainly due to the friction of the circulating fluid. If  $\Delta P_b$  is negligible, or if it is well known, the measurement of the mass flow and of the inlet and outlet temperature allows calculating the source power.

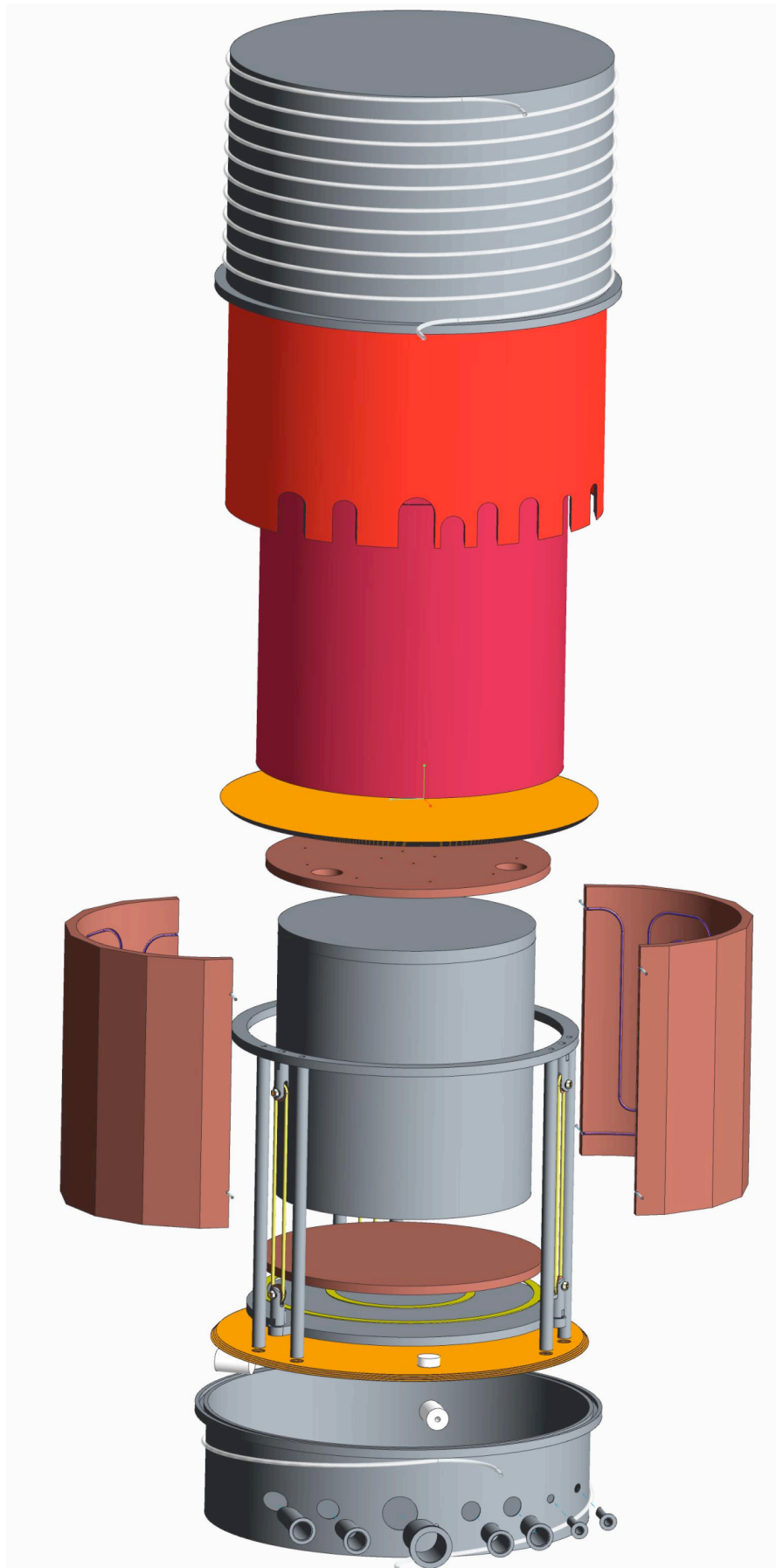


**FIG. 2:** Exploded view of the designed calorimeter.

In order to minimize  $\Delta P_b$ , the calorimeter is inserted in a vacuum chamber with thermal radiation shields. For the same purpose, the source and the heat exchanger are suspended using Kevlar ropes. Fig. 2 shows an exploded view of the designed calorimeter.

Precision measurements (within  $10^{-3}$ ) are required for water inlet and outlet temperature as well as for water mass flow: the temperature measurements will be carried out using platinum thermometer inserted in suitable pits where the flowing water is previously mixed to avoid temperature gradients while the flow is measured via Coriolis mass flowmeter.

As the power generated by the source decays exponentially, an accurate measurement of the activity must take into account the diffusion of heat in the massive radioprotection shield which causes a delay in the measurement. The problem can be analytically faced using a simple unidimensional model. Let us suppose an infinite plate of thickness  $L$ , having one side connected to a heat sink at temperature  $T_0$  and the other side heated by a time depending power per unit area:

$$\frac{P_g}{A} = \frac{P_0}{A} e^{-t/\tau}$$

The diffusion equation and the boundary conditions are:

$$\left\{ \begin{array}{l} \frac{\partial^2 T}{\partial x^2} = \frac{1}{D} \frac{\partial T}{\partial t} \\ k \frac{\partial T}{\partial x} \Big|_{x=0} = \frac{P_0}{A} e^{-t/\tau} \\ k \frac{\partial T}{\partial x} \Big|_{x=L} = h(T \Big|_{x=L} - T_0) \end{array} \right.$$

where  $k$  and  $D$  are the thermal conductivity and diffusivity, supposed constant,  $h$  is the heat exchange coefficient between the system and the thermostat. The asymptotic solution, corresponding to dynamic equilibrium, can be obtained by solving the equation by separation of variables:

$$T(x,t) = -\frac{P_0 \sqrt{\tau D}}{Ak} e^{-t/\tau} \left[ \frac{c_1}{c_2} \cos\left(\frac{x}{\sqrt{\tau D}}\right) + h\sqrt{\tau D} \sin\left(\frac{x}{\sqrt{\tau D}}\right) \right] + T_0$$

where 
$$\frac{c_1}{c_2} = \frac{\cos\left(\frac{L}{\sqrt{\tau D}}\right) + h\sqrt{\tau D} \sin\left(\frac{L}{\sqrt{\tau D}}\right)}{\sin\left(\frac{L}{\sqrt{\tau D}}\right) - h\sqrt{\tau D} \cos\left(\frac{L}{\sqrt{\tau D}}\right)}.$$

The power per unit area at  $x=L$  is:

$$\frac{P_m}{A} = h(T|_{x=L} - T_0) = \frac{P_g}{A} e^{-t_d/\tau} = \frac{P_0}{A} e^{-(t-t_d)/\tau}$$

where

$$t_d = \tau \cdot \ln \left( \cos \frac{L}{\sqrt{\pi D}} - \frac{k}{h\sqrt{\pi D}} \sin \frac{L}{\sqrt{\pi D}} \right).$$

Therefore, when the dynamic equilibrium is reached, the power generated by the source is measured by the calorimeter after a time interval  $t_d$ . If the heat diffuses fast, i.e. for large values of  $D$ , the delay tends to zero.

## 2.1 Estimation of measurement errors $\Delta P_r$

If the coolant is water around room temperature, the specific heat capacity is not temperature dependent (within 1‰) and eq. (2) can be rewritten as:

$$P_g = \dot{m} C_{H_2O} (T_{out} - T_{in}) + \Delta P_b \quad (3)$$

The temperature measurement is done with very precise thermometers, calibrated to achieve an error of  $\Delta T = \pm 5$  mK, whilst the water flux measurements is done with an error of  $\pm 0.1\%$  of the measured flux ( $\Delta \dot{m} = \pm 10^{-5}$  kg/s). The total measurement error  $\Delta P_m$  is then given by:

$$\Delta P_r = \Delta \dot{m} C_{H_2O} (T_{out} - T_{in}) + 2\Delta T \dot{m} C_{H_2O} = \begin{cases} \pm 1.4 \text{ W} & \text{if } P_g \cong 1000 \text{ W} \\ \pm 0.9 \text{ W} & \text{if } P_g \cong 500 \text{ W} \end{cases} \quad (4)$$

## 2.2 Estimation of dissipations and losses

In view of the large precision which will be required for the calorimetric measurement, 1% of the generated power, it is crucial to provide a reliable estimation of dissipations and losses. As mentioned before, the main source of dissipations is the friction of the circulating water, whilst sources of losses are thermal radiation in the vacuum chamber, conduction through the residual gas, conduction through the Kevlar suspension ropes and conduction through the measurements wires. In the next paragraphs, all these sources of dissipations and losses will be estimated at the maximum envisaged generated power, 1000 W.

### 2.2.1 Dissipation by friction of the circulating fluid

The starting point for the evaluation of the power generated by friction of the circulating water is the determination of the Reynolds number  $Re$ :

$$Re = \frac{vD}{\eta} = \frac{\dot{m}}{\frac{\pi}{4} D^2 \delta} \frac{D}{\eta} = \frac{4}{\pi} \frac{\dot{m}}{D \delta \eta} \quad (5)$$

where  $v$  is fluid velocity,  $\eta$  is the kinematics viscosity,  $\dot{m}$  is the fluid mass flow,  $\delta$  is the water density and  $D$  is the pipe inner diameter. Since the kinematics viscosity ranges from  $10^{-6}$  m<sup>2</sup>/s at  $T=20^\circ\text{C}$  to  $0.658 \cdot 10^{-6}$  m<sup>2</sup>/s at  $T=40^\circ\text{C}$ , with  $\dot{m} = 0.01$  kg/s and  $D=5$  mm we get:

$$2500 < Re < 4000 \quad (6)$$

Since a fluid flow is laminar if  $Re < 2320$  and turbulent if  $Re > 2320$ , result in (6) let us conclude that in the designed heat exchanger the flux will be turbulent. From the Reynolds number it is possible to calculate the friction coefficient, which is  $\lambda = 64/Re$  in case of laminar flux, whilst it is deducible from the following transcendent equation in case of turbulent flux:

$$\frac{1}{\sqrt{\lambda}} = -2 \log \left( \frac{2.51}{Re \sqrt{\lambda}} + 0.269 \frac{k}{D} \right) \quad (7)$$

where  $k$  is the inner rugosity of pipes. If  $k = 10 \mu\text{m}$ , we get  $\lambda = 0.048$  if  $Re = 2500$  and  $\lambda = 0.042$  if  $Re = 4000$ . If  $\Delta p$  is the pressure drop, we can now calculate the dissipation by friction per unit length as:

$$\frac{\dot{Q}_{\text{fric}}}{L} = \frac{\dot{m}}{\delta} \frac{\Delta p}{L} = \frac{\dot{m}}{\delta} \frac{\lambda \delta v^2}{2D} = \frac{8 \dot{m}^3 \lambda}{\pi^2 D^5 \delta^2} = 0.01 \div 0.0125 \text{ W/m} \quad (8)$$

The net length of the heat exchanger is almost 13 m, which becomes 15 m when considering all the connections. This let us estimate  $\dot{Q}_{\text{fric}} \approx 0.15 \div 0.2 \text{ W}$ .

### 2.2.2 Losses by thermal radiation

The losses due to heat exchanged by radiation between two surfaces,  $A$  in area, at the temperatures  $T_1$  and  $T_2$  respectively, are given by:

$$\dot{Q}_{\text{rad}} = \sigma \varepsilon A (T_2^4 - T_1^4) \quad (9)$$

where  $\varepsilon$  is the emissivity of the surfaces and  $\sigma = 5.67 \times 10^{-8} \text{ W/m}^2/\text{K}^4$  is the Stefan–Boltzmann constant. In our particular case, considering that the radiating surfaces are not at constant temperature and that several electro-polished copper screens ( $\varepsilon = 0.03$ ) have been introduced in the vacuum chamber to bring down the losses, eq. (9) can be re-written as:

$$\dot{Q}_{\text{rad}} = \frac{\sigma \varepsilon A}{n+1} (\langle T_2^4 \rangle - \langle T_1^4 \rangle) \quad (10)$$

where  $n$  is the number of copper screens ( $n = 8$  on top and side and  $n = 5$  on the bottom of the calorimeter). Three different components can be calculated: the heat exchanged by radiation by the bottom surface,  $\dot{Q}_{\text{rad bot}}$ , by the lateral surface,  $\dot{Q}_{\text{rad side}}$ , and by the top surface,  $\dot{Q}_{\text{rad top}}$ .  $\langle T_2^4 \rangle$  in the three cases have been estimated by finite element analysis at the maximum power of 1000 W in steady state conditions (see §4.6.1). To be conservative, we assumed that on the bottom surface  $\langle T_1 \rangle = 18^\circ\text{C}$  (the calorimeter is in contact with the ground), whilst on the top and side surface  $\langle T_1 \rangle = 25^\circ\text{C}$  (the vacuum tank is externally wrapped by a serpentine where the warm water getting out from the calorimeter flows). These considerations lead to:

$$\begin{aligned} \dot{Q}_{\text{rad bot}} &= \sigma \varepsilon \frac{0.26}{6} (9.5 \cdot 10^9 - 7.2 \cdot 10^9) = 0.17 \text{ W} \\ \dot{Q}_{\text{rad side}} &= \sigma \varepsilon \frac{1.09}{9} (1 \cdot 10^{10} - 7.9 \cdot 10^9) = 0.43 \text{ W} \\ \dot{Q}_{\text{rad top}} &= \sigma \varepsilon \frac{0.26}{9} (1 \cdot 10^{10} - 7.9 \cdot 10^9) = 0.10 \text{ W} \\ \dot{Q}_{\text{rad}} &= \dot{Q}_{\text{rad bot}} + \dot{Q}_{\text{rad side}} + \dot{Q}_{\text{rad top}} = 0.7 \text{ W} \end{aligned} \quad (11)$$

Considering the uncertainties of these estimations, it is safer to apply a factor of 2 to the results in eq. (11), concluding that:

$$\dot{Q}_{\text{rad}} = \dot{Q}_{\text{radbot}} + \dot{Q}_{\text{radside}} + \dot{Q}_{\text{radtop}} \lesssim 1.4 \text{ W} \quad (12)$$

This safety factor takes also into account the losses by conduction through the copper screen spacers, which are very difficult to be estimated.

### 2.2.3 Losses by conduction through the residual gas in the vacuum chamber

In the hypothesis to get a pressure in the vacuum chamber  $p \approx 10^{-4}$  mbar, the mean free path of air molecules is nearly 0.5 m, so much larger than the distance between the heat exchanger and the vacuum tank. The conduction through the residual gas is then in molecular regime, so that:

$$\dot{Q}_{\text{gas}} = \alpha A \left( \frac{\gamma + 1}{\gamma - 1} \right) \sqrt{\frac{R}{8\pi M \langle T \rangle}} p (T_2 - T_1) \quad (13)$$

where  $\alpha$  is a multiplicative factor ( $\alpha \approx 0.8$  for air at 300 K),  $A$  is the total exchange surface in  $\text{cm}^2$  ( $A \approx 2 \text{ m}^2$ ),  $\gamma$  is the ratio between the specific heat capacity at constant pressure and the specific heat capacity at constant volume ( $\gamma = C_p/C_v = 1.4$  for air),  $\sqrt{R/8\pi} = 0.2426$  to get  $\dot{Q}_{\text{gas}}$  in watts,  $M$  is the molecular weight in g/mole ( $M = 28 \times 0.8 + 32 \times 0.2 = 28.8$  g/mole for air),  $p$  is the pressure in mmHg ( $p = 10^{-4}$  mbar  $= 0.75 \cdot 10^{-4}$  mmHg),  $\langle T \rangle$  is the average temperature of the residual gas in kelvin and  $(T_2 - T_1)$  is the temperature variation between warm and cold surfaces. If we suppose that  $\langle T \rangle = 30^\circ\text{C}$  and  $(T_2 - T_1) \approx 20^\circ\text{C}$ , we get  $\dot{Q}_{\text{gas}} \approx 0.37 \text{ W}$ . Considering the uncertainties on temperatures and pressure, it is safer to apply a factor of 2 to this result concluding that:

$$\dot{Q}_{\text{gas}} \lesssim 0.75 \text{ W} \quad (14)$$

It is worth noting that  $\dot{Q}_{\text{gas}}$  is directly proportional to  $p$ , so that it is crucial to keep the vacuum pressure as low as possible. In particular, if  $p = 10^{-3}$  mbar the conduction through the residual gas is still in molecular regime (the mean free path of air molecules is nearly 5 cm), so eq. (13) still applies and  $\dot{Q}_{\text{gas}} \approx 3.7 \text{ W}$ , without considering any safety factor. As it will be clear in the next paragraph, such a value would strongly affect our possibilities to measure the power generated by  $^{144}\text{Ce}$  within 1%.

### 2.2.4 Losses by conduction through the Kevlar suspension ropes

In order to minimize the losses by conduction, the source is not in contact with the ground, but it is suspended by Kevlar ropes (see Fig. 2). The heat lost by conduction through the Kevlar ropes is then given by:

$$\dot{Q}_{\text{kevlar}} = k_{\text{kevlar}} \frac{A_{\text{kevlar}}}{L_{\text{kevlar}}} \Delta T \lesssim 0.01 \text{ W} \quad (15)$$

knowing that the thermal conductivity of Kevlar is  $k_{\text{kevlar}} = 4 \text{ W/m/K}$ ,<sup>17</sup> the total area of the three ropes is  $A = 24 \text{ mm}^2$ , the rope length is  $L = 300 \text{ mm}$  and the temperature gradient is

$\Delta T=20^{\circ}\text{C}$ . As expected, this result let us conclude that the losses by conduction through the Kevlar suspension ropes are negligible.

### 2.2.5 Losses by conduction through the measurement wires

By applying the usual safety factor, the heat losses by conduction through about  $n=40$  copper wires 0.2 mm in diameter and 10 cm long if  $\Delta T\sim 25^{\circ}\text{C}$  are given by:

$$\dot{Q}_{\text{wires}} = 2 \cdot n \cdot k_{\text{Cu}} \frac{A_{\text{wires}}}{L_{\text{wires}}} \Delta T \lesssim 0.25 \text{ W} \quad (16)$$

where  $k_{\text{Cu}}=390 \text{ W/m/K}$  is the thermal conductivity of copper.

### 2.2.6 Estimation of the total contribution $\Delta P_b$

Being aware of the risks implicit in the subtraction of two systematic errors, we could estimate the total contribution  $\Delta P_b$  to the generated power in eq. (2) at the envisaged maximum power, 1000 W:

$$\Delta P_b [P_g \approx 1000 \text{ W}] \approx \max(\dot{Q}_{\text{rad}} + \dot{Q}_{\text{gas}} + \dot{Q}_{\text{wires}}) - \min(\dot{Q}_{\text{fric}}) = 2.3 \text{ W} \quad (17)$$

This operation is not totally meaningless because the resulting  $\Delta P_b$  is not around zero, but the positive term is always much larger than the negative term. Considering that  $\dot{Q}_{\text{rad}}$  depends on the fourth power of temperature, whilst  $\dot{Q}_{\text{gas}}$  and  $\dot{Q}_{\text{wires}}$  depends linearly on the temperature gradient, a conservative estimate of the total losses at a generated power of 500 W is

$$\Delta P_b [P_g \approx 500 \text{ W}] \approx \frac{\max(\dot{Q}_{\text{rad}} + \dot{Q}_{\text{gas}} + \dot{Q}_{\text{wires}})}{2} - \min(\dot{Q}_{\text{fric}}) = 1.1 \text{ W} \quad (18)$$

## 3 SYSTEM LAY-OUT

The source lay-out is schematically shown in Fig. 3. It is made by a compacted cerium oxide powder contained in a double stainless steel case. The source is inserted in a biological shield, i.e. a tungsten alloy container 190 mm thick in the radial direction. The tungsten shield is made by three pieces, the main body, the internal plug and the upper cap. Due to its design, the bottom surface of both plug and cap are in direct contact with the main body. The other surfaces of the biological shield are not in direct contact one to each other and air gaps between them have been designed. The water path in the heat exchanger is schematically represented in Figs. 5 and 6. Water pipes are embedded in a 20 mm thick copper structure.

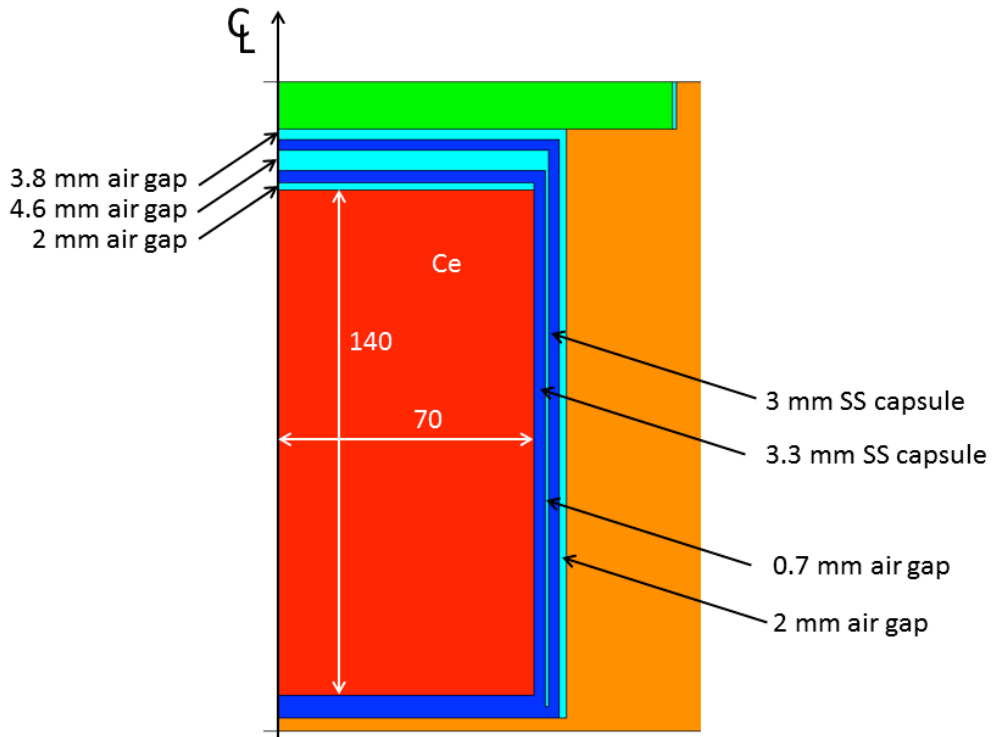


**FIG. 3:** Cerium oxide source dimensions. Cerium oxide is represented in red, stainless steel in blue, air in light blue, tungsten in green and orange.

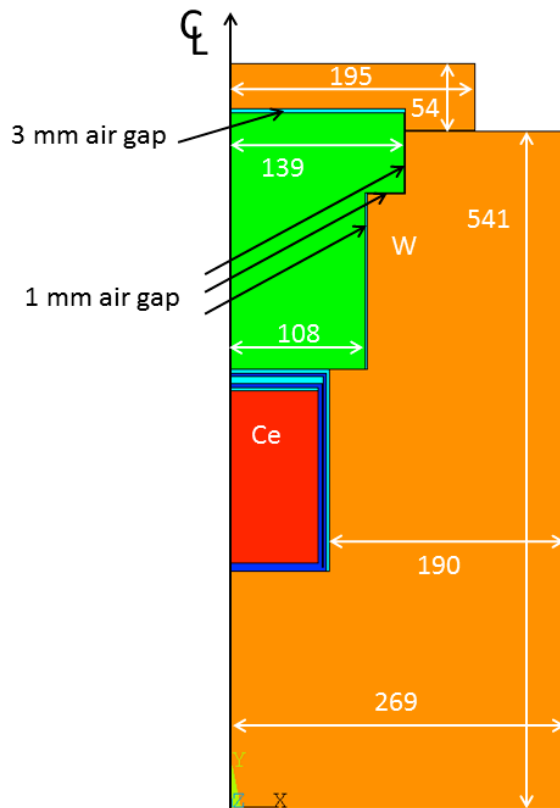


**FIG. 4:** Tungsten shield dimensions. Cerium oxide is represented in red, stainless steel in blue, air in light blue, tungsten in green and orange.

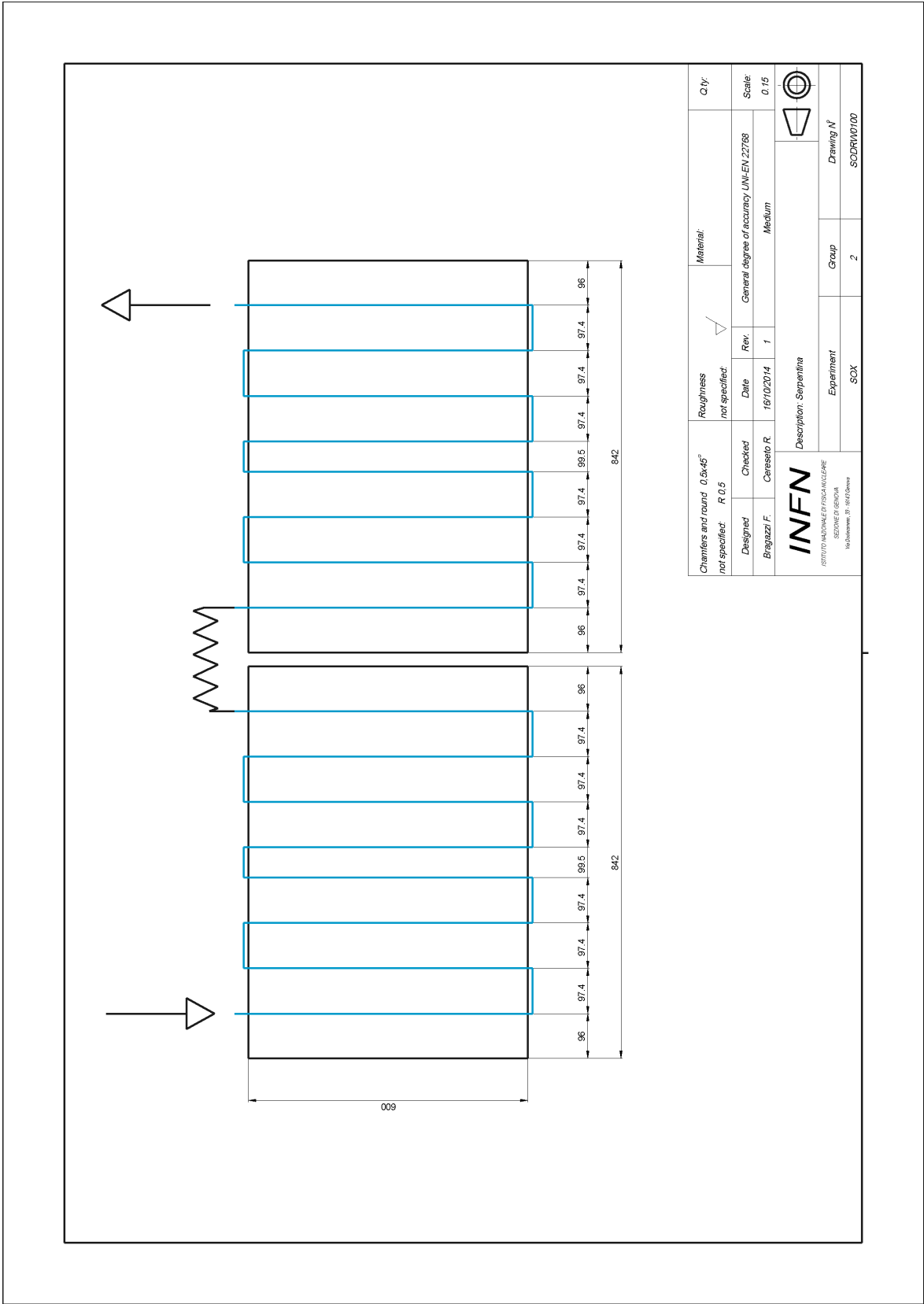


**FIG. 5:** Schematic representation of the water pipes in the later heat exchanger.

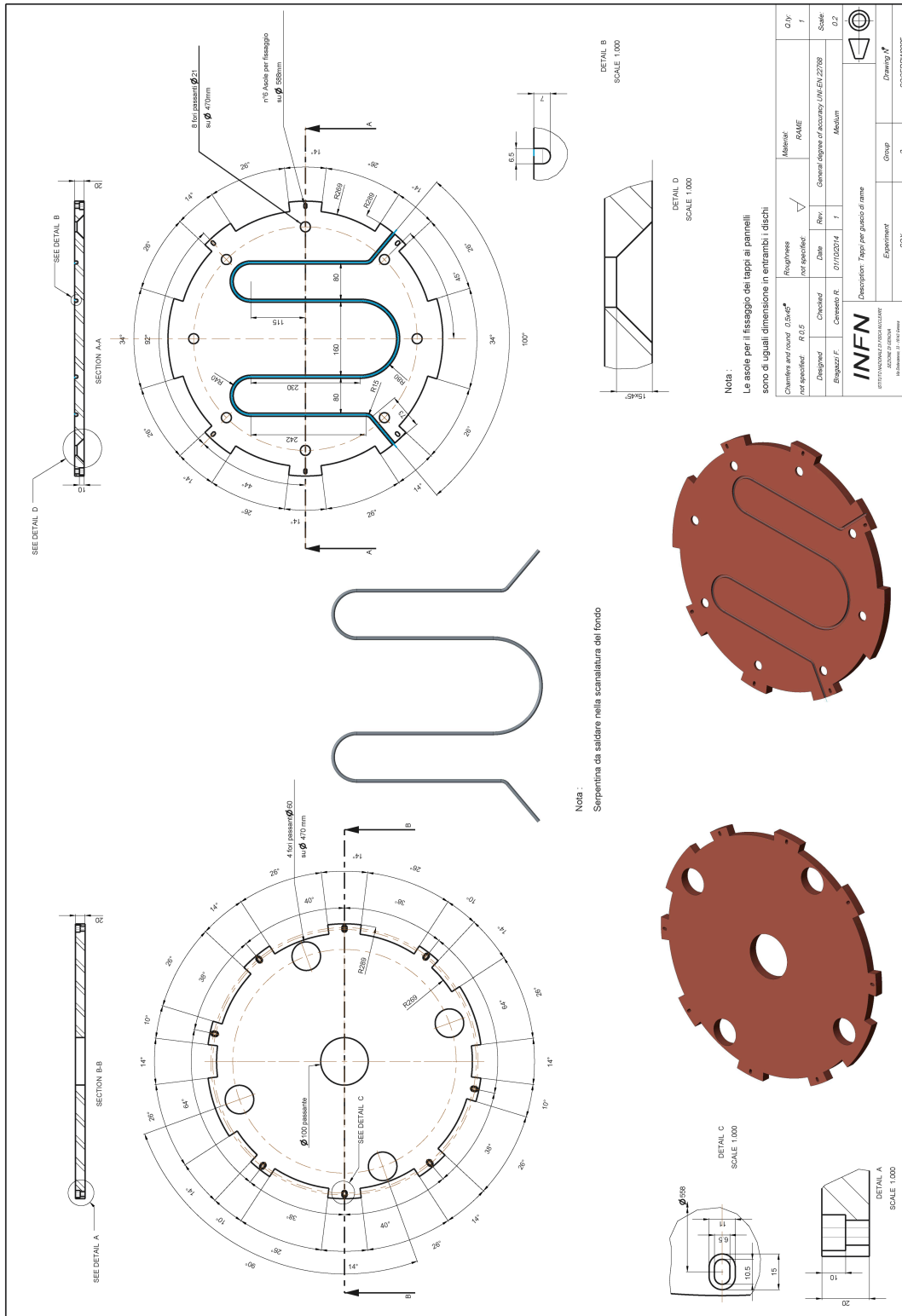


FIG. 6: Drawing of top and bottom covers of the heat exchanger, including water pipes.

#### 4 MATERIAL PROPERTIES

Reference properties of the source materials are the same as in (4) and are listed in Table 1. The only uncertain properties are those of the cerium oxide powder. Several considerations, based on different measurements<sup>4</sup>, let us set the thermal conductivity to the constant value of 4 W/m/K, whilst the minimum density after compaction is known to be 4000 kg/m<sup>3</sup>.

Reference emissivity values, needed to take into account the heat exchange by thermal radiation, are shown in Table 2. Radiative effects are present in all closed air gaps and also on the surfaces exposed to external environment. In this last case the ambient temperature is supposed to be 38°C. Table 2 also lists the reference film coefficients needed to take into account the heat exchanged by natural convection by the surfaces exposed to external environment. Typical values of free convection in air range from 5 to 25 W/m<sup>2</sup>/K, so we adopted a conservative criterion and choose film coefficients around 5 W/m<sup>2</sup>/K. The ambient temperature is again considered to be 38°C.

**TAB. 1:** Reference material properties

Material	Thermal conductivity (W/m/K)	Specific heat (W/kg/K)	Density (kg/m <sup>3</sup> )
Cerium oxide	4	368	4000
Stainless steel	14.0+0.015·T(°C)	467	7930
Tungsten	70	156	18460
Air	0.025+6.94·10 <sup>-5</sup> ·T(°C)	1000	1
Copper	386	380	8954
Water	0.58	4190	1000

**TAB. 2:** Reference emissivities and film coefficients

Interface	Emissivity	Film coefficient (W/m <sup>2</sup> /K)
Cerium oxide/stainless steel	0.9	–
Stainless steel/ stainless steel	0.4	–
Stainless steel/tungsten	0.4	–
Tungsten/tungsten	0.5	–
Tungsten/copper	0.5	–
Stainless steel/infinity (T <sub>air</sub> =38 °C)	0.4	7
Tungsten/infinity (T <sub>air</sub> =38 °C)	0.5	5
Copper/infinity (T <sub>air</sub> =38 °C)	0.5	5

## 5 FINITE ELEMENT MODELS

The layout of the  $\text{CeO}_2$  source within its biological shield is perfectly axisymmetric, so in principle it is possible to perform a 2-dimensional (2D) axisymmetric finite element analysis, which would be completely equivalent to the 3-dimensional (3D) one. Unfortunately, the heat exchanger shape breaks this symmetry and demands for a fully 3D FE model. In order to have consistent results, all finite element models are then 3-dimensional.

In Figs. 7, 8 and 9 the finite element mesh of  $\text{CeO}_2$  source, W shielding and heat exchanger is shown. In full symmetry, it contains 603000 nodes and 606000 elements. To maximize the accuracy of the calculations, the models have been meshed as regularly as possible. Regions with dissimilar mesh patterns have been tied together by generating constraint equations that connect the nodes of one region to the elements of the other region. The behavior of water is taken into account using a special element, FLUID116, which has the ability to conduct heat and transmit fluid between its two primary nodes.

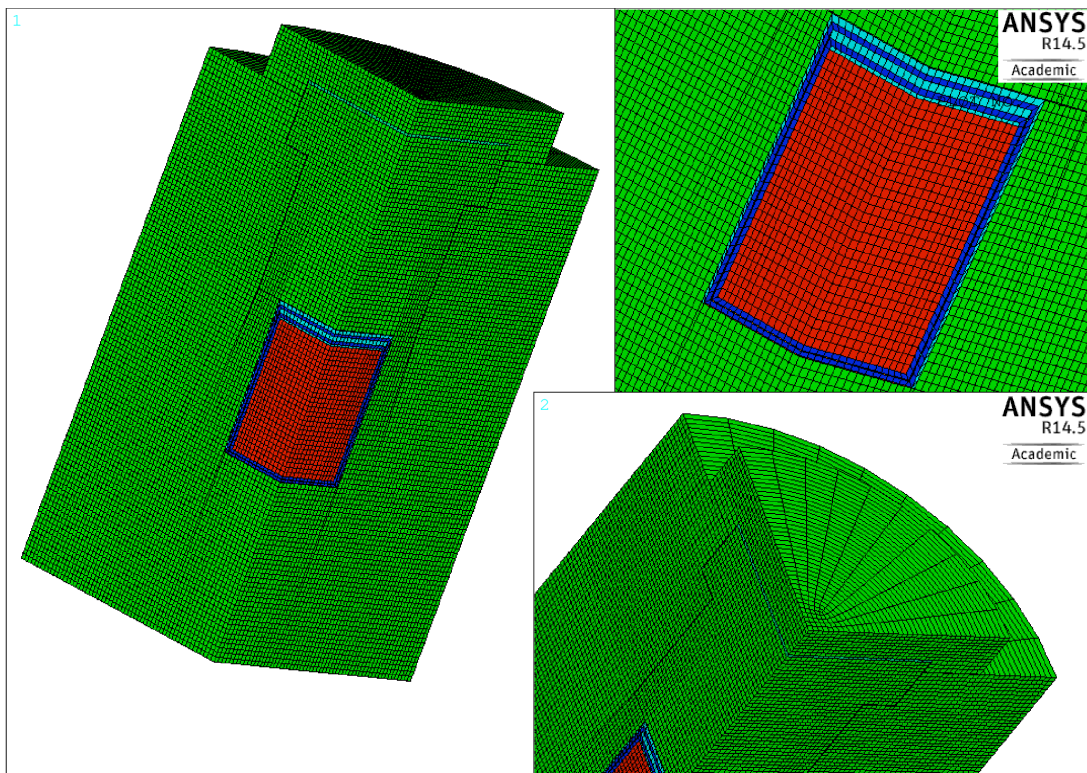


**FIG. 7:** Finite element model of the Ce source inside the biological shield.

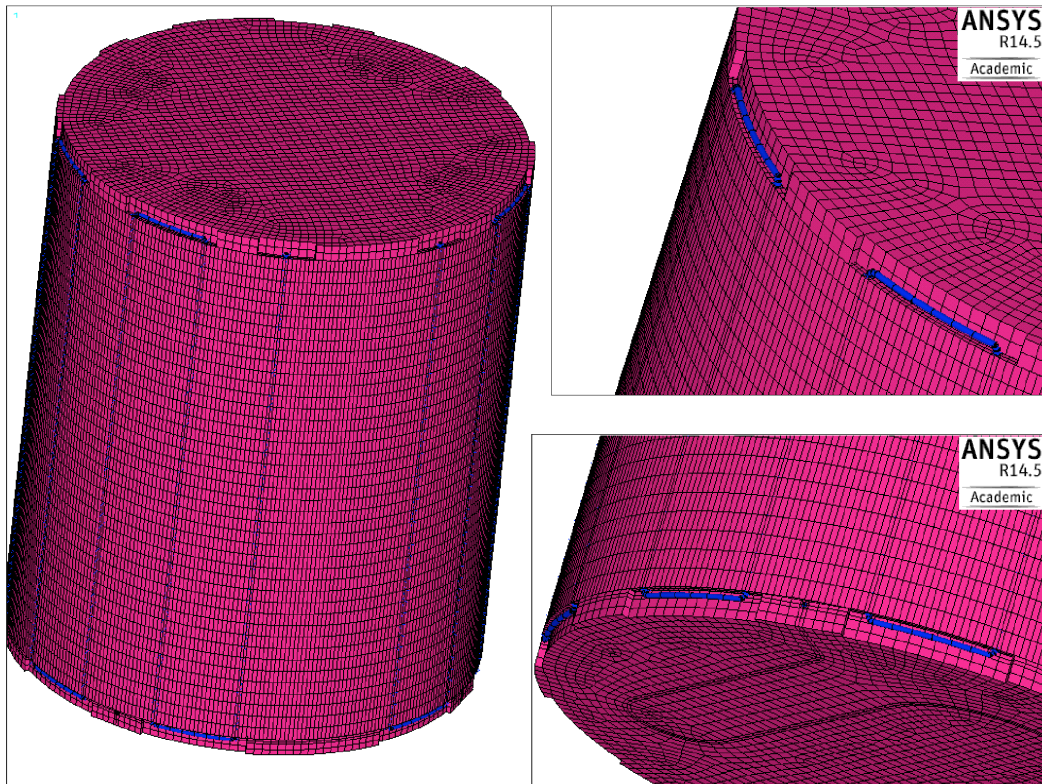


**FIG. 8:** Finite element model of the heat exchanger.

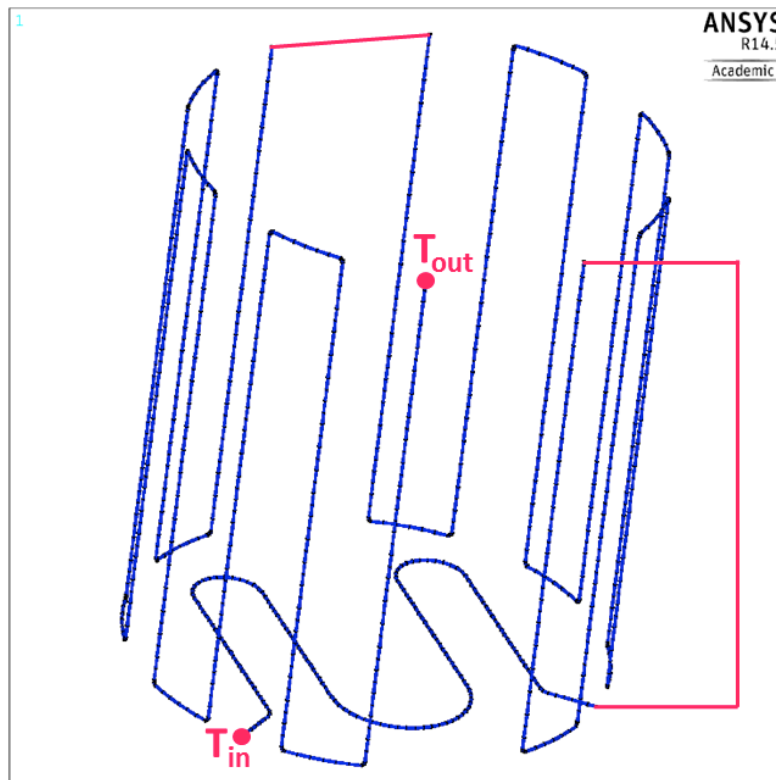


**FIG. 9:** Water flow in the heat exchanger.

## 6 FINITE ELEMENT ANALYSES

Several finite element analyses have been carried out to understand the thermodynamic behavior of this complex system. They are:

- (1) Steady state thermal analysis of the standalone  $\text{CeO}_2$  source
- (2) Steady state thermal analysis of the  $\text{CeO}_2$  source inside the biological shielding
- (3) Transient thermal analysis of the  $\text{CeO}_2$  source inside the biological shielding (results of the steady state analysis of the standalone  $\text{CeO}_2$  source used as initial conditions)
- (4) Steady state thermal analysis of the source cooled by water flow
- (5) Transient thermal analysis of the source cooled by water flow (results of the steady state analysis of the  $\text{CeO}_2$  source inside the biological shielding used as initial conditions)

In any conditions the temperature of stainless steel case shall not overcome  $800^\circ\text{C}$ , the temperature of tungsten shielding shall not overcome  $200^\circ\text{C}$  and the temperature of any part exposed to the environment shall not overcome  $120^\circ\text{C}$ . The maximum temperature of water, when the cooling system is active, shall not overcome  $80^\circ\text{C}$ , in order to guarantee not to have vapor bubbles in the fluid.

The source activity is supposed to be uniform in the  $\text{CeO}_2$  volume and non-penetrant, i.e. the power is dissipated in the  $\text{CeO}_2$  volume only. This condition is not realistic but does not affect the steady state calculations and is conservative in the transient analysis. The nominal dissipated power for steady state analyses is supposed to be  $1000\text{ W}$ . In transient analyses it decays following the exponential law  $P = P_0 e^{-t/\tau}$ , where  $P_0=1000\text{ W}$  and  $\tau=411$

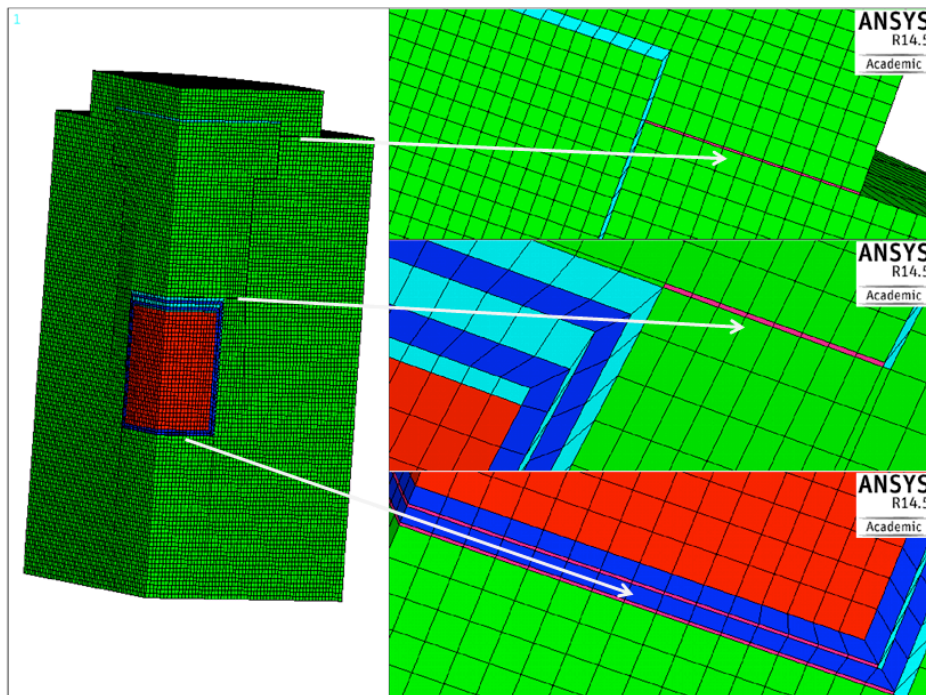


**FIG. 10:** Dummy materials where thermal conductivity can be reduced with respect to nominal value to simulate worsened contact conditions.

days, corresponding to a half-life of 284.893 days.

Contact between surfaces is considered perfect. In order to take into account worsened conditions, special volumes have been modeled at interfaces, where thermal conductivities can be reduced with respect to their nominal values (see Fig. 10).

Radiation towards the environment and convection, where considered, are applied on all external surfaces, including the bottom ones, i.e. both standalone source and shielded source are supposed to be suspended. This condition is worse from a thermal point of view than the conduction through any kind of support base.

## 6.2 Standalone CeO<sub>2</sub> source

The standalone CeO<sub>2</sub> source is analyzed in steady state conditions only, as we ignore the procedure, and the corresponding boundary and initial conditions, followed in Mayak to

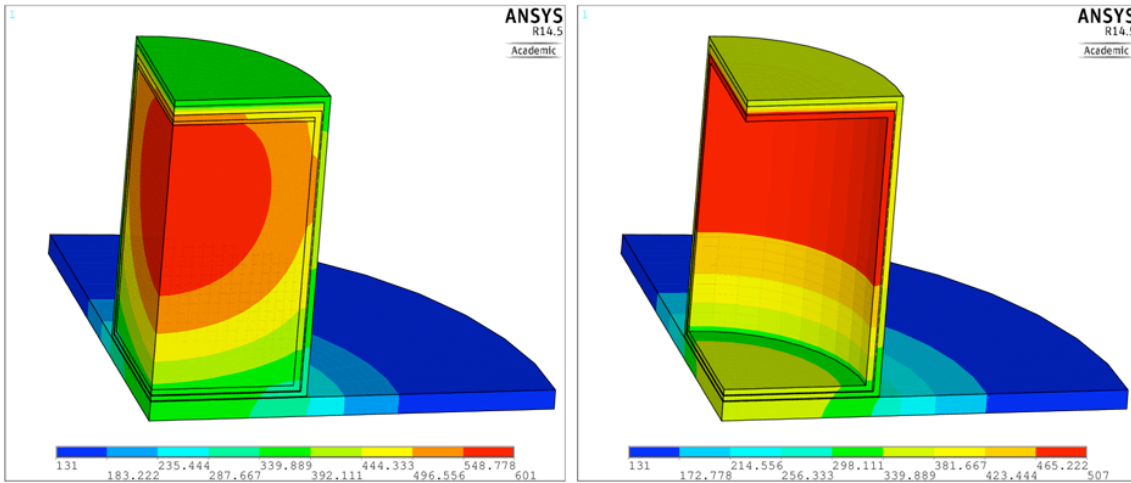


**FIG. 11:** Temperature map of the whole source (left) and hiding the Ce elements (right) using the material properties listed in Tables 1 and 2 resulting from the steady state analysis of the standalone source.

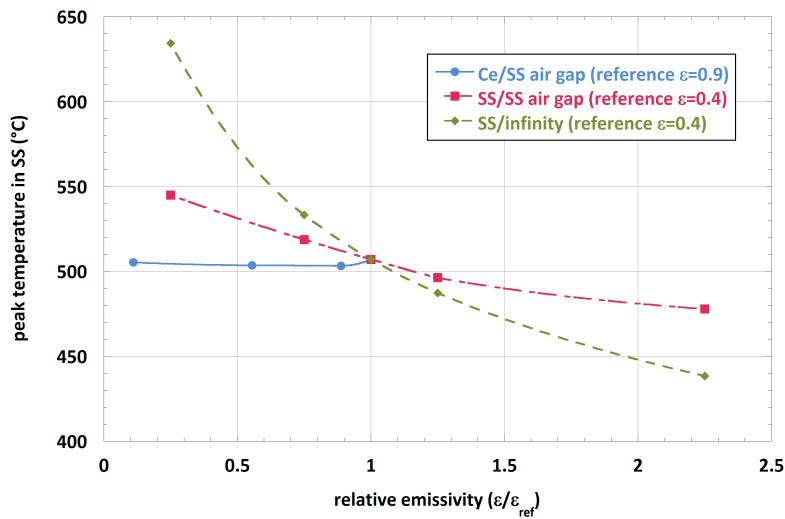


**FIG. 12:** Peak temperature in stainless steel as function of emissivity relative to its reference value resulting from the steady state analysis of the standalone source. The plot is obtained by changing emissivity one by one and keeping the others to their reference values.

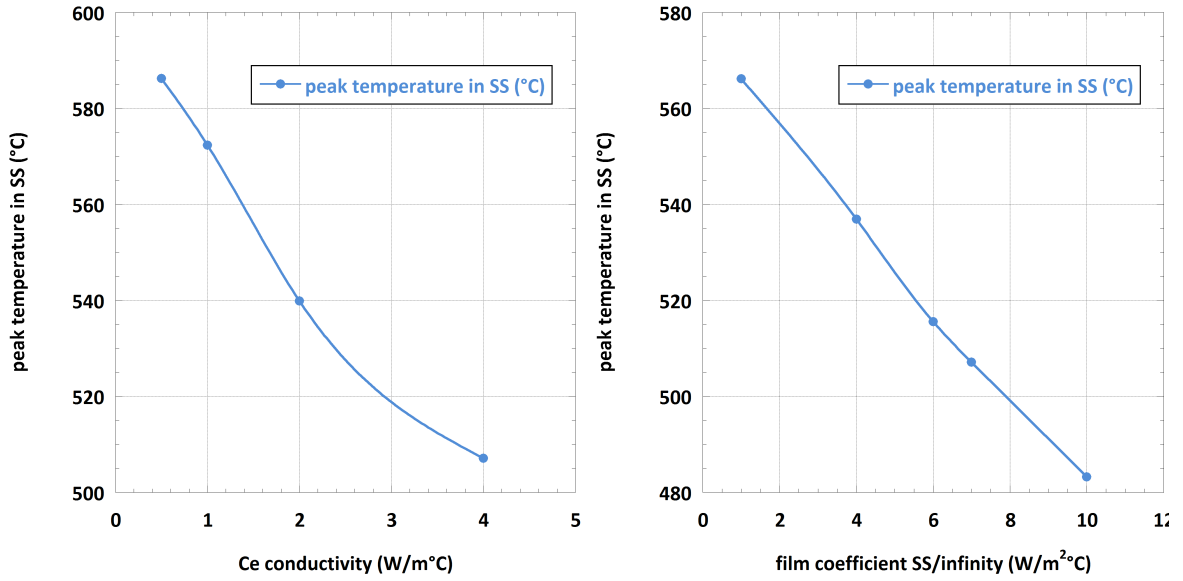


**FIG. 13:** Peak temperature in stainless steel as function of Ce conductivity (left) and convection film coefficient between stainless steel and environment (right) resulting from the steady state analysis of the standalone source.

assemble it.<sup>15</sup> When outside the biological shielding, the source lies down on a stainless steel disk, 400 mm in diameter and 10 mm thick. When the input material properties are those listed in Table 1, with emissivities in air gaps and film coefficient for convection on the external surfaces of stainless steel as listed in Table 2, the temperature map corresponding to 1000 W of dissipated power in CeO<sub>2</sub> is shown in Fig. 11. The peak temperature in stainless steel is 507°C, well below the limit of 800°C.

Since some of the material properties have a non negligible degree of uncertainty, we let them vary one by one to understand their effect on the system, and in particular the effect on the stainless steel peak temperature. Fig. 12 shows the peak temperature in stainless steel as function of emissivity relative to its reference value, obtained by changing the emissivities one by one and keeping the others to their reference values. Fig. 13 shows the peak temperature in stainless steel obtained by varying CeO<sub>2</sub> conductivity and convection film coefficient between stainless steel and environment. As expected, in steady state, none of these dependences seems to be particularly critical as the peak temperature in stainless steel remains well below the imposed limit of 800°C. Also, nothing relevant can be detected by reducing the thermal conductivity of contact materials (see Fig. 10) up to a factor of 10. We do expect a heavier impact of material properties variations on the transient behavior.

### 6.3 Shielded CeO<sub>2</sub> source

The CeO<sub>2</sub> source positioned inside its tungsten biological shielding is analyzed in steady state and transient conditions. Input material properties are those listed in Table 1, with emissivities in air gaps and film coefficient for convection on the external surfaces of tungsten as listed in Table 2. No calculations have been performed by varying material properties: in steady state we do not expect to get different results with respect to those found

for the standalone source, whilst the effects on the transient behavior are not particularly significant.

### 3.6.1 Steady state analysis

The temperature map of  $\text{CeO}_2$  source and tungsten shielding is shown in Fig. 14. Once inserted in the biological shielding, the peak temperature of cerium oxide reduces to  $510^\circ\text{C}$

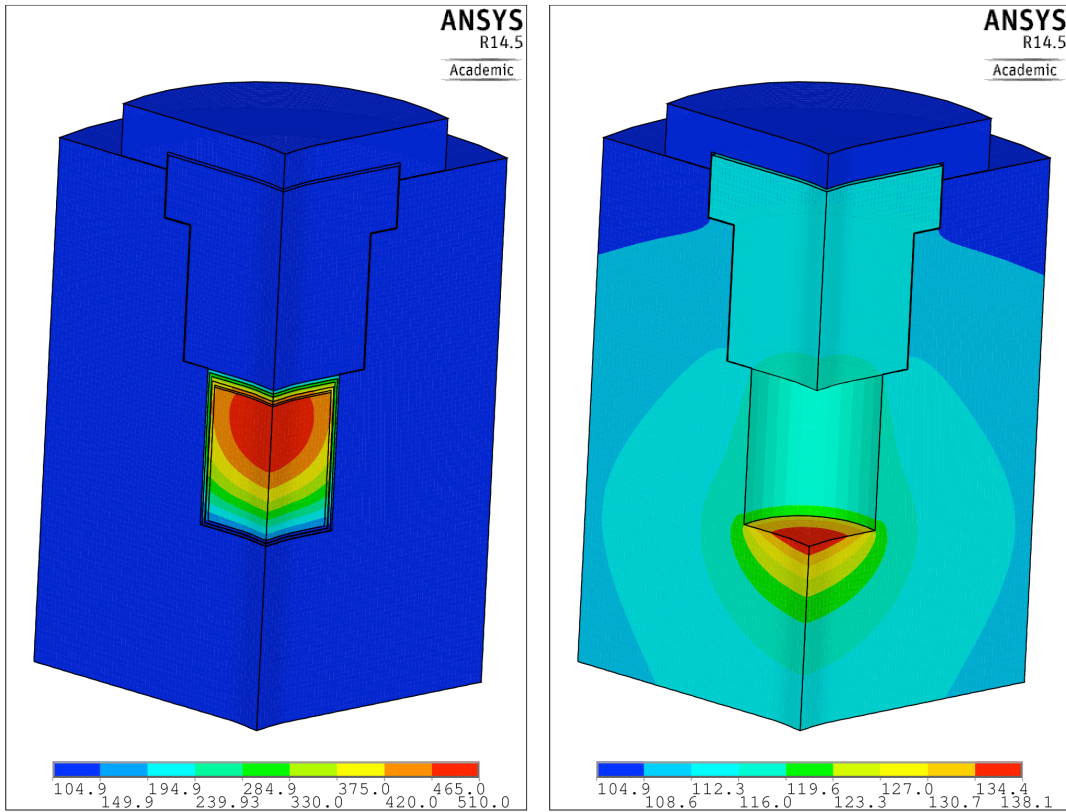


**FIG. 14:** Temperature maps of the Ce source inside the biological shielding (left) and of the shielding itself (right) resulting from the steady state analysis of the shielded source.

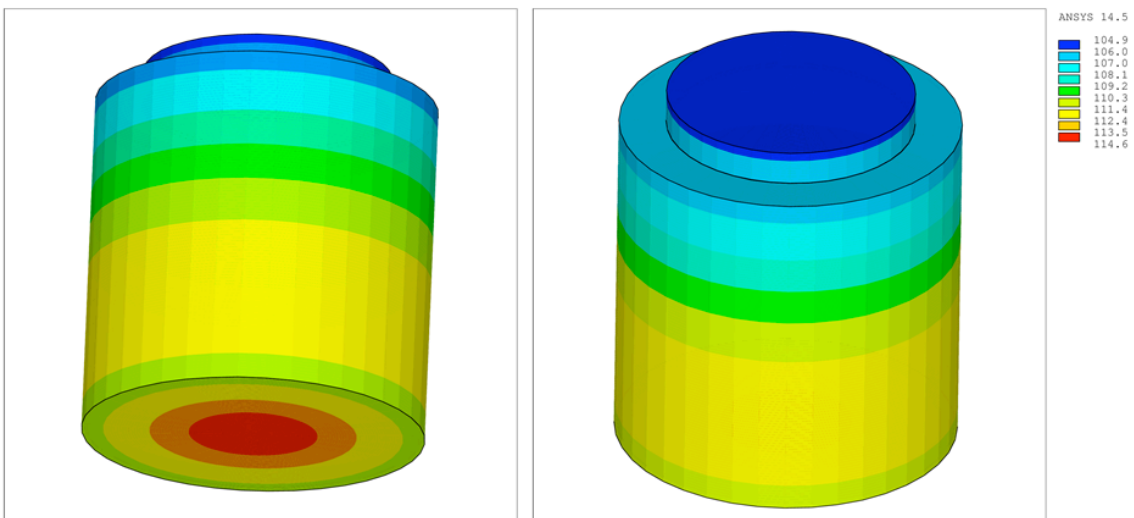


**FIG. 15:** Temperature maps on the external surface of the biological shielding resulting from the steady state analysis of the shielded source.

and the peak temperature in tungsten grows up to 138°C, well below the 200°C limit. The temperature on the external surface of the biological shielding is quite high. It ranges from 105°C and 115°C, still within reasonable limits for handling.

### 3.6.2 Transient analysis

As mentioned in the previous paragraphs, the transient analysis has been carried out by dissipating a power  $P = P_0 e^{-t/\tau}$  ( $P_0=1000$  W and  $\tau=411$  days) in the cerium oxide elements. The initial conditions of the transient analysis are the temperature maps resulting from the previous analysis for the standalone CeO<sub>2</sub> source (cerium oxide, stainless steel case and internal air gaps) and a uniform temperature distribution at 38°C for the tungsten shield.

Fig. 16 shows the peak temperature in cerium oxide, tungsten and on the shield external

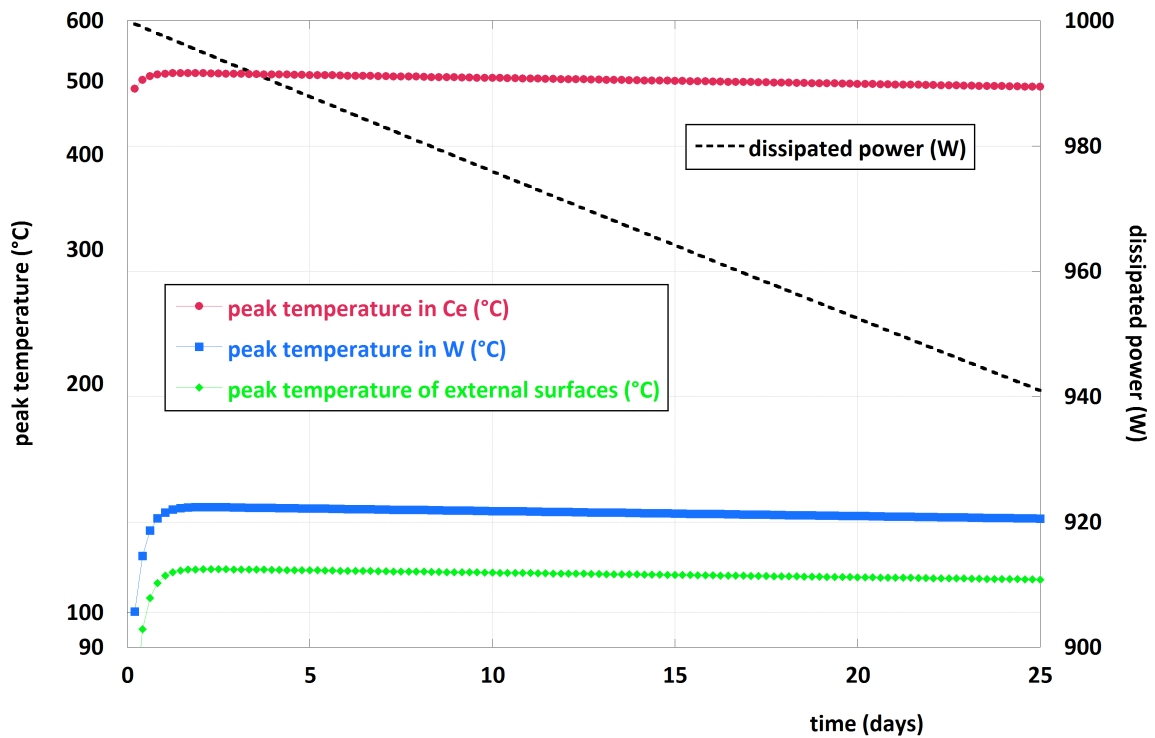


**FIG. 16:** Peak temperature in in cerium oxide, tungsten and on the external surfaces as function of time together with the dissipated power resulting from the transient analysis of the shielded source.

surfaces as function of time together with the dissipated power. As expected, after an initial transient, all those temperatures decay following exactly an exponential law (a straight line in logarithmic scale). The transient lasts nearly 2 days in cerium oxide, 2.5 days in tungsten and 2.5 days externally.

## 6.4 Cooled CeO<sub>2</sub> source

The CeO<sub>2</sub> source cooled by forced water flow, as shown in Figs. 8 and 9, is analyzed in steady state and transient conditions. Input material properties are again those listed in Table 1, with emissivities in air as listed in Table 2.

### 4.6.1 Steady state analysis

As in the previous arrangements, the steady state analysis is performed by dissipating  $P_0=1000$  W within the CeO<sub>2</sub> source. Setting the inlet temperature at  $T_{in}=18^\circ\text{C}$  and the water flow at  $\dot{m}=0.01$  kg/s, the outlet temperature  $T_{out}$  can be easily found as:

$$P_0 = \dot{m}C(T_{out} - T_{in}) \Rightarrow T_{out} = \frac{P_0}{\dot{m}C} + T_{in} = 41.86635^\circ\text{C} \quad (19)$$

where  $C=4190$  W/kg/K is the specific heat of water. We are clearly ignoring any kind of thermal loss: our assumption is that either they are negligible or they are not negligible but we accurately measure them in the test phase of the calorimeter, so that they can be added as in (2) to get the power generated by the source. The outlet temperature as calculated by the finite element analysis is  $T_m=41.86694^\circ\text{C}$ , corresponding to a “measured” power of:

$$P_m = \dot{m}C(T_m - 18) = 1000.025 \text{ W} \quad (20)$$

This implies an accuracy of 25 ppm on the energy balance calculations, at least in steady state conditions. Here and in the next paragraphs, we indicate the power calculated via eq. (20) as measured power,  $P_m$ , as it is determined using the temperature difference between outlet and inlet, i.e. the quantity we are going to measure through the calorimeter.

Figs. 17 and 18 show the temperature of water resulting from the steady state analysis. It is worth noting that the maximum temperature of water is  $44.3^\circ\text{C}$ , slightly higher than the outlet temperature. Also, most of the water temperature gradient, from  $18^\circ$  to  $\sim 40^\circ\text{C}$ , takes place in the bottom part of the heat exchanger, whilst the side elements stays between  $40^\circ\text{C}$  and  $45^\circ$ . This is true also for the copper in the heat exchanger, so that we do expect that most of the losses due to thermal radiation will be due to the small bottom area and not to the very large side area, contributing to the minimization of the losses.

Finally, as expected, activating the water cooling the peak temperatures of both CeO<sub>2</sub> source and tungsten shielding reduce, as shown in Fig. 20.

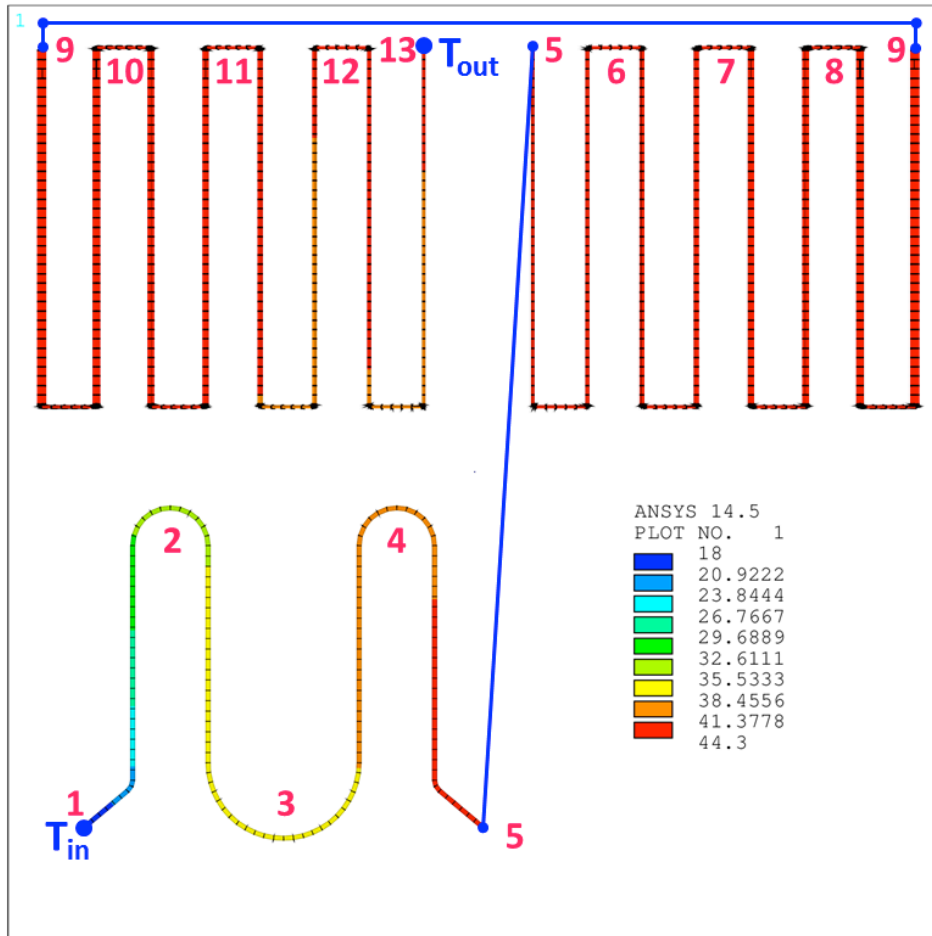


FIG. 17: Map temperature of water from steady state analysis.

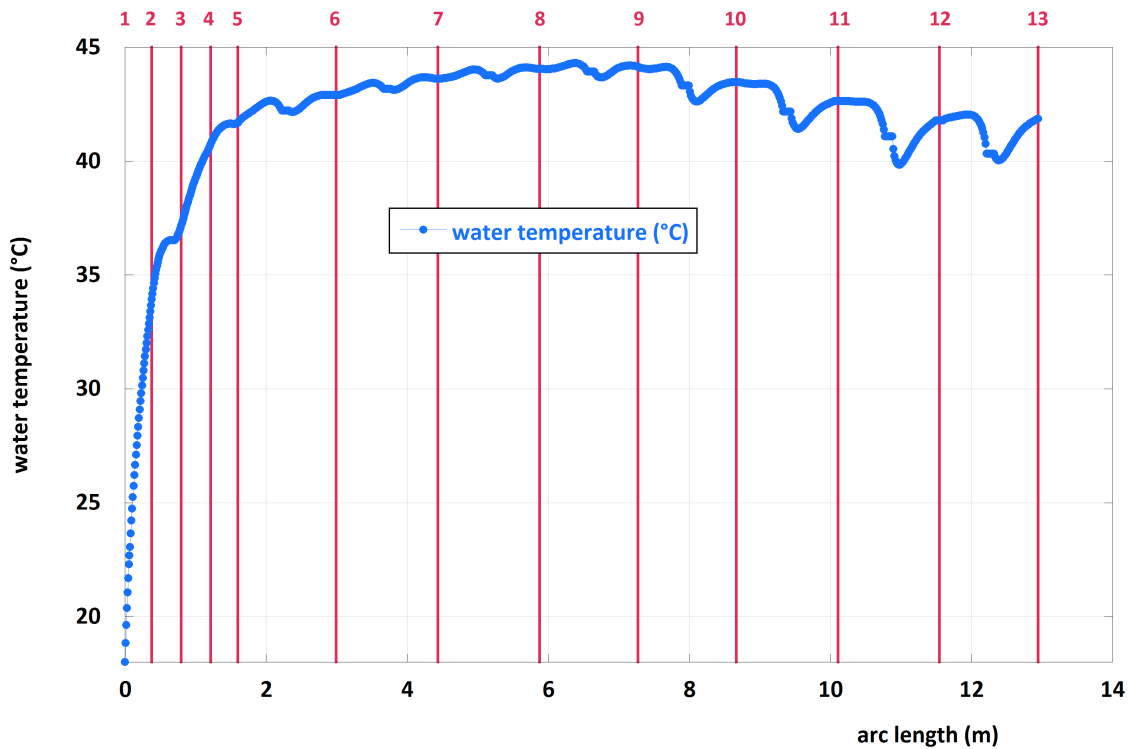


FIG. 18: Temperature of water as function of the pipe arc length, beginning at  $T_{in}$  and ending at  $T_{out}$ . Numbers indicate the locations as shown in Fig. 17.

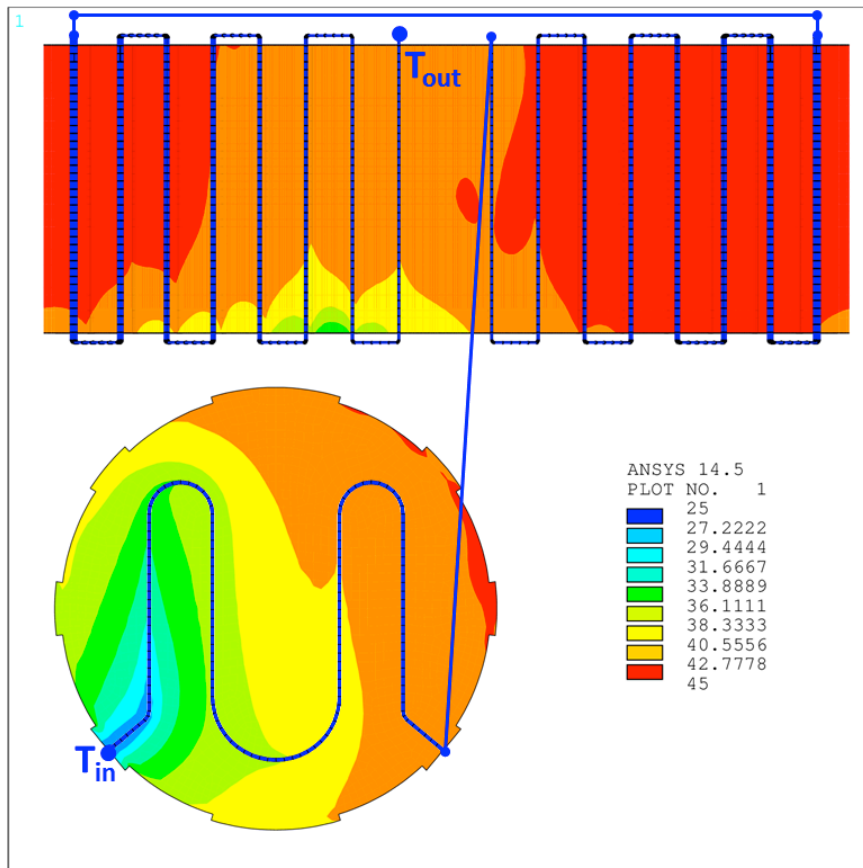


FIG. 19: Temperature of the copper heat exchanger.

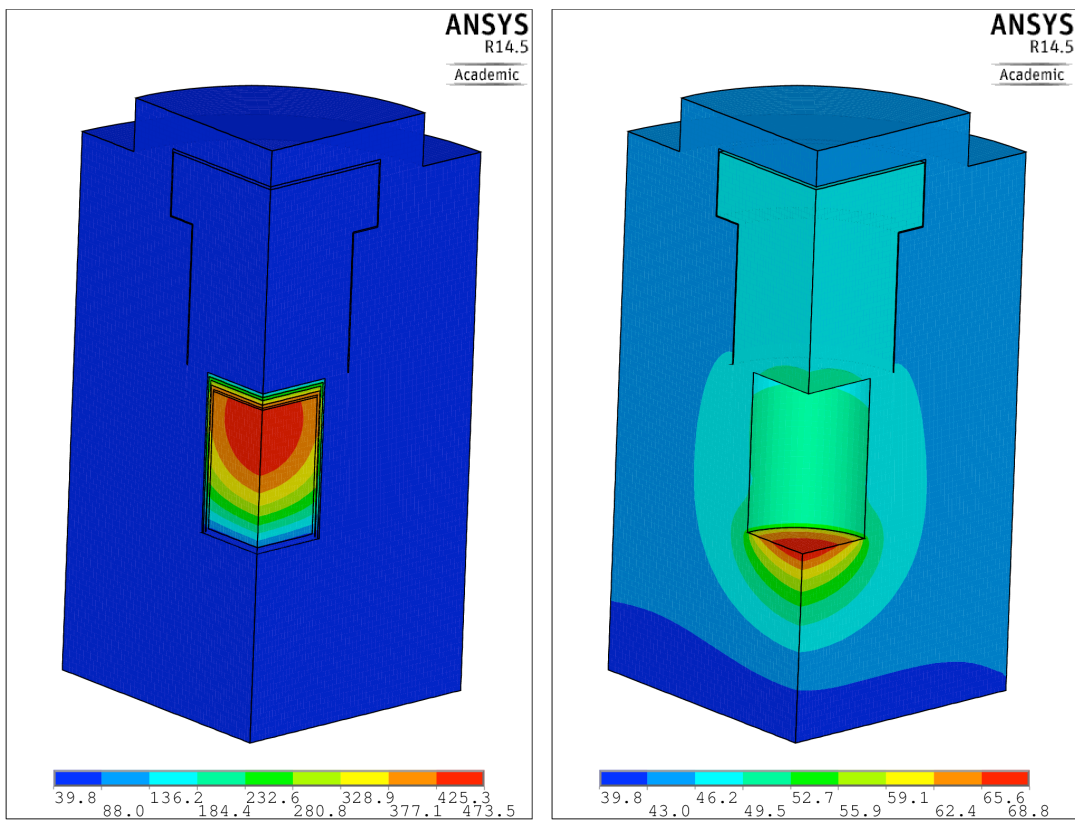


FIG. 20: Temperature maps of the Ce source inside the biological shielding (left) and of the shielding itself (right) resulting from the steady state analysis of the cooled source.

#### 4.6.2 Transient analysis

The transient analysis is again performed by dissipating the power  $P_g = P_0 e^{-t/\tau}$  ( $P_0=1000$  W and  $\tau=411$  days) in the cerium oxide elements. The initial conditions are the temperature maps resulting from the previous analysis for the shielded  $CeO_2$  source (cerium oxide, stainless steel case, tungsten shield and internal air gaps) and a uniform temperature distribution at  $38^\circ C$  for heat exchanger.

The main result of the transient analysis is the outlet temperature of water as function of time, which, via eq. (20), allows calculating the measured power. Fig. 21 shows the measured and the generated power as function of time. After an initial transient, which lasts nearly 1.5 days, the measured power follows the same simple exponential law as the generated power,  $P_m = P_{m0} e^{-t/\tau}$ . Fitting the data of the measured power, one finds  $P_{m0}=1000.5$  W, which corresponds to a relative difference with the generated power  $(P_m - P_g)/P_g = 500$  ppm. There is then a systematic difference which is  $\Delta P_d = 0.5$  W when  $P_g = 1000$  W, and  $\Delta P_d = 0.25$  W when  $P_g = 500$  W. This difference is not due to worsened calculation accuracy, but to the fact that the heat exchanger measures the generated power with a certain delay of time:

$$P_m = P_0 e^{-(t-\Delta t)/\tau}, \quad \Delta t = \tau \ln \frac{P_{m0}}{P_m} = 0.2 \text{ days} \quad (21)$$

which is due to the inertia of the system to transfer heat from the cerium oxide inside to the heat exchanger outside. Luckily, this delay is very small if compared to the  $^{144}Ce$  decay time (411 days), so that if we completely neglect it, the precision of the measured power is 0.05%, well below to the required precision of 1%.

Recalling the results in §0 and §2.2.6 for  $\Delta P_r$  and  $\Delta P_b$  respectively, we can estimate the error on the measurements as:

$$\Delta P_m \approx \Delta P_r + \Delta P_b + \Delta P_d = \begin{cases} 4.25 \text{ W} & \text{if } P_g \approx 1000 \text{ W} \\ 2.25 \text{ W} & \text{if } P_g \approx 500 \text{ W} \end{cases} \quad (22)$$

which in percentage becomes:

$$\frac{\Delta P_m}{P_m} \approx \begin{cases} 0.43\% & \text{if } P_g \approx 1000 \text{ W} \\ 0.45\% & \text{if } P_g \approx 500 \text{ W} \end{cases} \quad (23)$$

The conclusion is that in the range of generated power between 500 W and 1000 W the error on the measurement seems to be safely within the required 1%.

In order to get a precise estimation of the transient duration, it is useful to plot the relative difference between the measured power and the shifted exponential law  $P_0 e^{-(t-\Delta t)/\tau}$ , with  $P_0=1000$  W and  $\Delta t=0.2$  days, as shown in Fig. 22. To be conservative, it is reasonable to set that the transient duration corresponds to a relative difference between the measured power and the shifted exponential law ranging from 10 to 50 ppm. Then, the transient lasts for a period between 1.7 and 2 days.

In order to give an evaluation of the calculation accuracy, we can use the maximum oscillation of the  $P_m$  data with respect to the best fit exponential curve. Such an oscillation, less than 3 ppm in absolute value, should be added to the uncertainty on the measured power

as calculated in steady state condition, 25 ppm, to get a guessed accuracy of the finite element analysis of about 30 ppm.

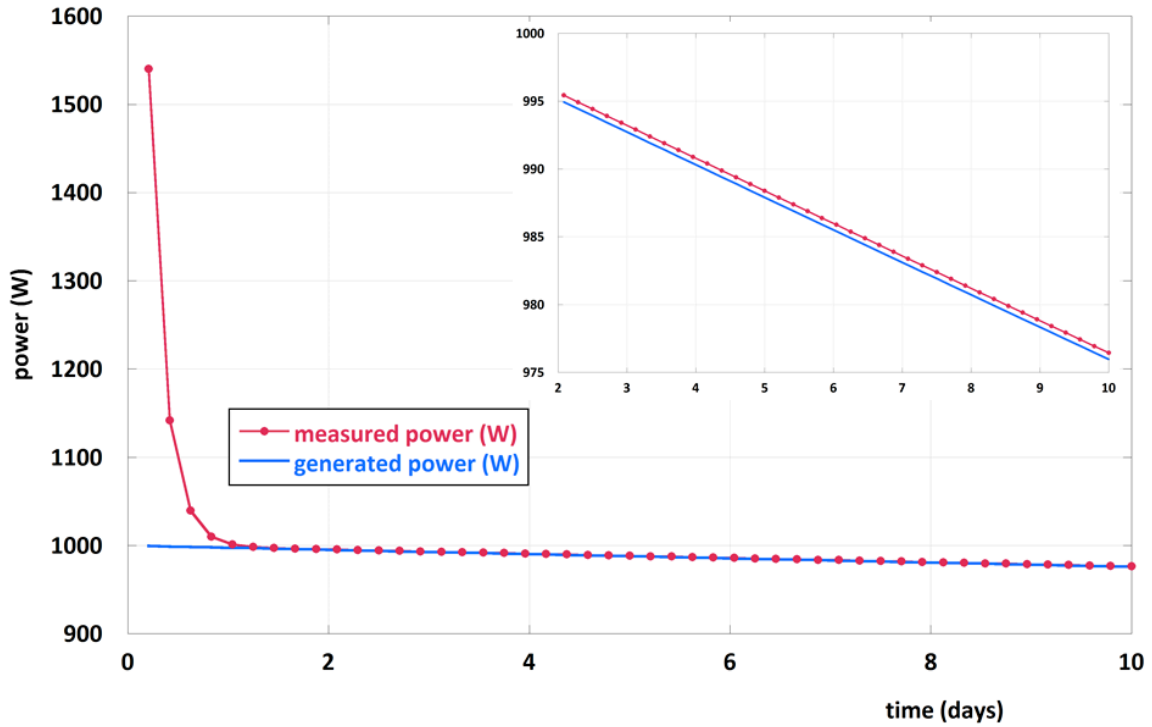


**FIG. 21:** Measured and generated power as function of time.

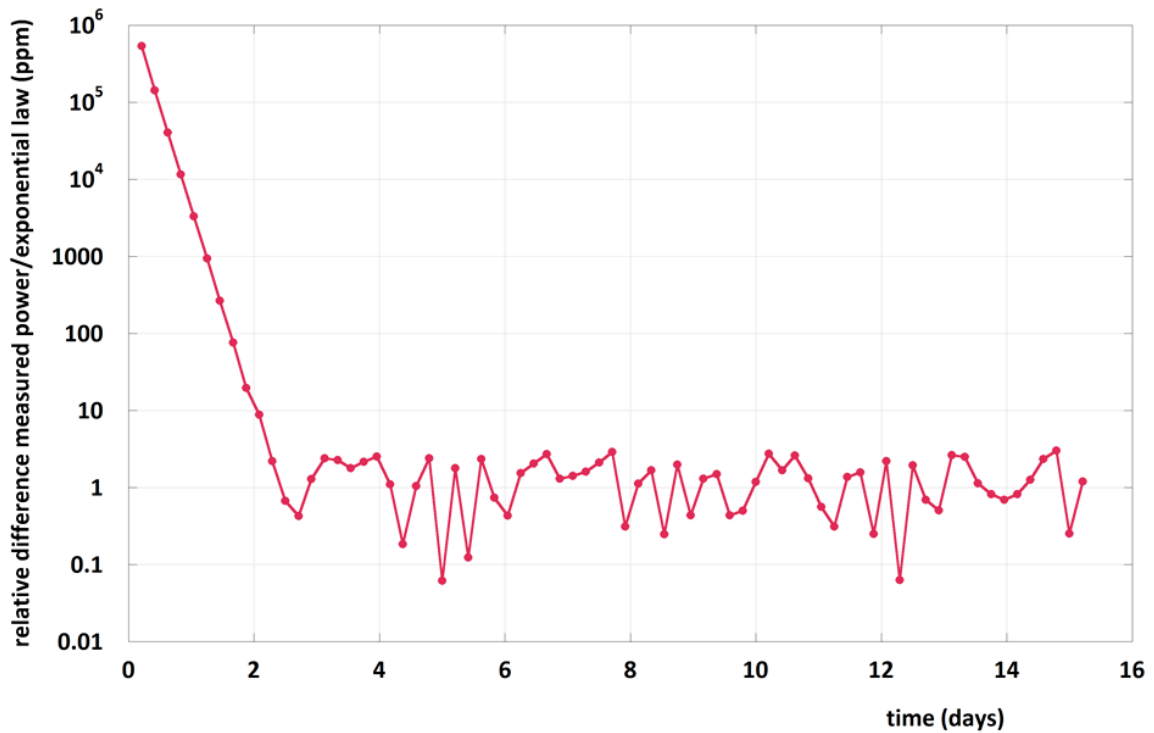


**FIG. 22:** Relative difference in absolute value between the measured power and the shifted exponential law  $P_0 e^{-(t-\Delta t)/\tau}$  with  $P_0=1000$  W and  $\Delta t=0.2$  days.

## 7 CONCLUSIONS

A flow calorimeter was designed with the aim to measure the activity of the antineutrino source of the SOX experiment with accuracy better than 1%. The thermal finite element analyses have allowed the optimization of the heat exchanger and an evaluation of the effect related to the heat diffusion in the massive biological shield.

## 8 REFERENCES

- (1) G.Bellini *et al.*, “SOX: Short distance neutrino Oscillations with BoreXino”, J. High Energy Phys. **8** 38 (2013), doi: 10.1007/JHEP08(2013)038.
- (2) A.Aguilar *et al.*, LSND Collaboration, Phys. Rev. D **64** 112007 (2001).
- (3) A.Aguilar *et al.*, MiniBooNE Collaboration, Phys. Rev. Lett. **110** 161801 (2013).
- (4) C.Giunti and M.Laveder, Phys.Rev. C **83** 065504 (2011).
- (5) G.Mention *et al.*, Phys. Rev. D **83** 073006 (2011).
- (6) A.Mueller *et al.*, Phys. Rev. C **83** 054615 (2011).
- (7) C.Giunti *et al.*, Phys. Rev. D **88** (2013).
- (8) G.Bellini *et al.*, Phys. Rev. D **89** 112007 (2014).
- (9) G.Bellini *et al.*, Nature **512**, 383–386 (28 August 2014).
- (10) G.Bellini *et al.*, Physics Letters B **722** (2013) 295–300.
- (11) P.Yala and D. Leterme, “CeSOX: études thermiques pour la sécurité de l’expérience”, CEA Technical Note DEN/DANS/DM2SSEMT/BCCR/NT/14-011/A (2014).
- (12) [www.ansys.com](http://www.ansys.com).
- (13) Plan IRFU “CeLAND 144Ce Source –Source 75 kCi – Capsule” N° 71 3139 DM – 2100 000 PC
- (14) G.Ventura and V.Martelli, “Thermal conductivity of Kevlar 49 between 7 and 290 K”, Cryogenics 49 (2009) 735–737, doi: 10.1016/j.cryogenics.2009.08.001.